# Elastic breakup cross sections of well-bound nucleons

K. Wimmer,[1,2] D. Bazin,[2] A. Gade,[2,3] J. A. Tostevin,[2,4] T. Baugher,[2,3] Z. Chajecki,[2] D. Coupland,[2,3] M. A. Famiano,[5]
T. K. Ghosh,[6] G. F. Grinyer,[7] M. E. Howard,[8] M. Kilburn,[2,3] W. G. Lynch,[2,3] B. Manning,[8] K. Meierbachtol,[2,9]
P. Quarterman,[2,3] A. Ratkiewicz,[2,3] A. Sanetullaev,[2,3] R. H. Showalter,[2,3] S. R. Stroberg,[2,3] M. B. Tsang,[2] D. Weisshaar,[2]
J. Winkelbauer,[2,3] R. Winkler,[2] and M. Youngs[2,3]

[1]*Department of Physics, Central Michigan University, Mt. Pleasant, Michigan 48859, USA*
[2]*National Superconducting Cyclotron Laboratory, Michigan State University, East Lansing, Michigan 48824, USA*
[3]*Department of Physics and Astronomy, Michigan State University, East Lansing, Michigan 48824, USA*
[4]*Department of Physics, Faculty of Engineering and Physical Sciences, University of Surrey, Guildford, Surrey GU2 7XH, United Kingdom*
[5]*Department of Physics, Western Michigan University, Kalamazoo, Michigan 49008, USA*
[6]*Variable Energy Cyclotron Centre, 1/AF Bidhannagar, Kolkata 700064, India*
[7]*Grand Accélérateur National d'Ions Lourds (GANIL), CEA/DSM-CNRS/IN2P3, Boulevard Henri Becquerel, 14076 Caen, France*
[8]*Department of Physics and Astronomy, Rutgers University, New Brunswick, New Jersey 08903, USA*
[9]*Department of Chemistry, Michigan State University, East Lansing, Michigan 48824, USA*

The $^9$Be($^{28}$Mg,$^{27}$Na) one-proton removal reaction with a large proton separation energy of $S_p(^{28}\text{Mg}) =$ 16.79 MeV is studied at intermediate beam energy. Coincidences of the bound $^{27}$Na residues with protons and other light charged particles are measured. These data are analyzed to determine the percentage contributions to the proton removal cross section from the elastic and inelastic nucleon removal mechanisms. These deduced contributions are compared with the eikonal reaction model predictions and with the previously measured data for reactions involving the removal of more weakly bound protons from lighter nuclei. The role of transitions of the proton between different bound single-particle configurations upon the elastic breakup cross section is also quantified in this well-bound case. The measured and calculated elastic breakup fractions are found to be in good agreement.

## I. INTRODUCTION

Nucleon removal reactions are a very effective means both to populate nuclei far from stability with relatively high yields and to probe their structure. The use of projectile beams of high energy allows thick reaction targets to be used, providing sufficient luminosity for precise measurements, even for very exotic systems. These high incident energies (few 100 MeV per nucleon) also allow certain simplifications in the theoretical description of the reaction dynamics, namely, the use of the sudden (fast collision) and eikonal (forward scattering) approximations. In general, three physical mechanisms may contribute to the one-nucleon removal reaction cross section. Their relative importance depends sensitively on the mass and charge of the target nucleus and the separation energy of the removed nucleon from the projectile ground state. In the case of very weakly bound nucleons and a heavy, highly charged target nucleus the reaction is often dominated by elastic Coulomb breakup and large soft-$E1$ excitation strength to low relative energy two-body states of the (residue + nucleon) breakup continuum; see, for example, Refs. [1,2] and references therein.

For light target nuclei, most often $^9$Be and $^{12}$C, and the removal of a more well-bound nucleon, which is our primary interest here, such Coulomb dissociation contributions are negligible and the reaction proceeds by the strong interaction. The two contributing mechanisms are then (i) elastic breakup of the projectile, also called diffraction dissociation, where the differential forces acting between the constituents and the target dissociate the projectile but leave the target nucleus

in its ground state, and (ii) inelastic breakup, where the interactions that remove the nucleon transfer energy to and remove the target nucleus from the elastic channel. This second mechanism is often called stripping. Since these two reaction mechanisms lead to distinct final states, their cross sections can be added and, since most intermediate-energy experiments measure only the projectile-like residues (after nucleon removal), these are normally compared with the sum of model calculations of the cross sections computed due to the two mechanisms. However, given the now significant body of experimental data that shows systematic differences of these measured removal yields from those calculated using shell-model plus reaction theory inputs, shown in Refs. [3,4], particularly those involving well-bound nucleons, the quality of the theoretical predictions of these two mechanisms is significant to validate the models used. We note that, in the case of a $^9$Be target, which is itself weakly bound with neutron separation energy $S_n = 1.66$ MeV and with no bound excited states, the stripping mechanism at energies near 100 MeV per nucleon will in general populate a many-particle final state and several light fragments, including the removed nucleon.

There have been extensive investigations of few-body models for the elastic breakup of the deuteron and well-clustered nuclei due to the Coulomb and nuclear interactions. Many have been extended, refined, and applied for the study of light weakly bound (halo) nuclei. These, in general, provide an excellent description of the increasing body of available elastic scattering and elastic breakup data on both one- and two-neutron halo systems. To account for the many-body nature of light halo nuclei, more microscopic and *ab initio*

structure-reaction treatments are also being developed. Few-body methods now include Faddeev-based, coupled-channels, and multiple-scattering quantum methods and eikonal-like and other semiclassical approaches, each optimal for different ranges of projectile energies and target nuclei but with valuable regions of overlap. In contrast, the reaction dynamics of elastic (and inelastic) breakup of more bound nucleons has received relatively little recent theoretical or experimental attention. Here, published calculations have been restricted to the use of eikonal models (e.g., [3,5,6] and multiple references therein) and the transfer to the continuum (TC) technique [7,8], although the latter is not applicable to proton removal and in its usual implementation uses approximations that are also poorly suited to reactions involving well-bound neutrons [9,10].

Early experimental studies of the removal reaction mechanism [11] also focused on the study of neutron removal from light neutron halo nuclei. In these experiments, neutron detectors covered only very forward angles and the elastic breakup component of the cross section was measured exclusively. Based on a quite simple geometrical model and the assumed dominance of the asymptotic region of the neutron wave function, it was suggested that the relative contribution to the removal reaction cross section from the diffractive mechanism will decrease with the neutron separation energy as $1/\sqrt{S_n}$—a relatively rapid fall in the diffraction component with $S_{n,p}$. Intermediate-energy eikonal model calculations for both well- and weakly bound nucleons on the other hand suggest that the single-particle removal cross sections (stripping plus diffraction) are strongly correlated with the root mean squared (rms) radius of the orbital from which the nucleon is removed; see, e.g., Fig. 2 of Ref. [3]. The calculations also suggest a weaker dependence of the elastic breakup contribution on separation energy and that this component persists and contributes significantly to the removal of well-bound nucleons. This paper aims to quantify this fractional elastic breakup contribution by using more exclusive measurements for the $^9$Be($^{28}$Mg,$^{27}$Na) one-proton removal reaction with proton separation energy $S_p(^{28}$Mg$) = 16.79$ MeV.

The first precise measurement of the individual contributions from the stripping and diffraction mechanisms to nucleon removal [12] also exploited weakly bound projectiles, $^8$B and $^9$C, having proton separation energies of $S_p = 0.137$ MeV and 1.296 MeV, respectively. The measured contributions from the diffractive and stripping mechanisms were found to be in good agreement with the predictions using the eikonal reaction dynamics description. That analysis also made use of continuum discretized coupled channels (CDCC) calculations of the elastic breakup to correct the measurements for the cross section that was unobserved due to the restricted solid angle coverage for proton and light charged particle detection in the experiment.

In this work, we extend this earlier study of exclusive reaction mechanism measurements to the removal of strongly bound protons. The data are compared with eikonal reaction model calculations and the role of transitions of the proton between bound single-particle configurations is quantified in this strongly bound case. We show conclusively that the importance of the elastic breakup mechanism is not limited

to loosely bound systems but persists in the removal of well-bound nucleons. The dependence of the elastic breakup fraction on $S_p$ will be discussed.

We study the $^9$Be($^{28}$Mg,$^{27}$Na) reaction that is well suited as a test case since (i) the proton separation energy from $^{28}$Mg is large ($S_p = 16.79$ MeV) and (ii) intense intermediate-energy beams of $^{28}$Mg are available. Furthermore, since both $^{28}$Mg and its reaction residue $^{27}$Na have a simple structure, due to the $N = 16$ subshell closure, their spectra are very well described by shell-model calculations in the $sd$-shell model space. Based on shell-model spectroscopy, the one-proton removal reaction from $^{28}$Mg is expected to mainly populate the $^{27}$Na ground state. No $\gamma$-ray detection was used to identify the $^{27}$Na final state in the present measurement. The new experimental data are compared with the earlier data for the loosely bound $^8$B and $^9$C systems [12].

## II. EXPERIMENTAL SETUP

The $^{28}$Mg beam was produced by fragmentation of an $^{40}$Ar primary beam with an energy of 140 MeV/u, provided by the coupled cyclotron facility at the National Superconducting Cyclotron Laboratory (NSCL), on a 846 mg/cm$^2$ $^9$Be production target. The desired fragment with an energy of 93 MeV/u was selected with the A1900 fragment separator [13] and impinged on a 9 mg/cm$^2$ $^9$Be secondary target at the target position of the S800 high-resolution magnetic spectrograph [14]. Incoming beam particles were identified event by event by their time of flight between two plastic scintillators before the target. The average rate on target was $5 \times 10^5$ $^{28}$Mg/s. The largest contaminant, $^{29}$Al, amounted to only 1.5% of the total beam intensity.

The reaction residues were identified by an energy-loss measurement in an ionization chamber in the focal plane detector box of the S800 spectrograph and the time of flight between a scintillator before the target and one in the focal plane. Momentum and energy of the reaction residues were reconstructed from the magnetic rigidity setting of the S800 spectrograph and the angles and positions of particles in the focal plane, measured with position-sensitive cathode readout drift chambers (CRDCs). Light charged particles from the removal reaction were detected in coincidence with the heavy $^{27}$Na residue in the high-resolution array HiRA [15]. $\Delta E$-$E$ telescopes based on 1.5-mm-thick double-sided silicon strip detectors (DSSSDs) and 4-cm-long CsI crystals allowed for unambiguous event-by-event identification of light charged particles, such as protons, deuterons, tritons, $^3$He, and $\alpha$ particles. The HiRA array covered polar angles ($\vartheta$) from 9° to 56° and, for a given value of $\vartheta$, up to 40% of the azimuthal angles were covered. A correction for the limited azimuthal acceptance within the $\vartheta$ range was applied following our previous work [16].

Two settings of the S800 spectrograph were used. Both optical settings have distinct advantages, which are described below. The first optics mode, (i), is the so-called focused mode. The second mode, (ii), the so-called dispersion matched mode, offers a higher resolution. In mode (i), in order to precisely measure the inclusive one-proton removal reaction cross section, the beam was focused on the target. Corrections for

the incoming momentum dispersion were made by measuring the position and angle at the intermediate image before the target with two position-sensitive parallel plate avalanche counters (PPACs). In the focused mode, acceptance cuts were limited and well under control. Since the reaction point on the target is well defined, the angle of the light charged particles could be determined with high precision. However, the momentum resolution for the heavy residues is then limited to $\Delta p = 24$ MeV/$c$. In mode (ii), in contrast to the high-resolution mode, the spectrograph was operated in the dispersion-matched mode, allowing for a precise measurement of the momentum change in the reaction ($\Delta p = 4.6$ MeV/$c$). The disadvantage of this method, since the dispersion of the beam at the target plane is very large, is that only part of the incoming beam hits the target. Thus, a measurement of the absolute reaction cross section cannot be obtained and only relative values are reported. A second, additional uncertainty in this measurement mode is the uncertainty in the event-by-event position of the reaction (in the dispersive direction) in the target plane. Since the beam is spread over the target, the emission angle of the light particle can only be obtained with a $\vartheta$ uncertainty of $6°$–$9°$, depending on the angle.

## III. EXPERIMENTAL DATA ANALYSIS

The inclusive one-proton removal reaction cross section was measured in the focused mode. No coincidence with particles detected in HiRA was required. Due to the finite acceptance of the S800 spectrograph, corrections at the largest and smallest residue momenta had to be applied. In total, these corrections amount to 2% of the inclusive cross section. For the $^9$Be($^{28}$Mg,$^{27}$Na) reaction an inclusive cross section of 36(1) mb was obtained.

In coincidence with the $^{27}$Na residue, light charged particles are detected in HiRA. Events with deuterons, tritons, or heavier particles are associated with the inelastic removal (stripping) mechanism since the additional nucleons can only originate from the target nucleus. Both elastic and inelastic removal processes contribute to events where $^{27}$Na nuclei and a proton are detected in coincidence. In elastic breakup events, the energy of the detected proton and that of the corresponding one-proton removal residue are correlated. This correlation can be investigated through the missing mass of the event, which is reconstructed from the momenta and energies (the momentum four-vectors $P$) of the $^{27}$Na residue and the proton:

$$M_{\text{miss}} = \sqrt{(P_{\text{beam}} + M_{\text{target}} - P_p - P_{\text{Na}})^2}.$$

This missing-mass spectrum is shown in Fig. 1(c). Figure 1 also presents the missing-mass spectra for the previously measured cases, weakly bound proton removal from the light nuclei $^8$B and $^9$C [12], for comparison with the present case. The elastic breakup events are characterized by the peak in the missing mass, corresponding to the mass of the target nucleus, $M(^9$Be$) = 8.395$ GeV/$c^2$. In the elastic breakup mechanism the nucleon is removed in a collision that leaves the target nucleus in its ground state. As no energy is lost to the target nucleus in this case, this leads to a sharp peak in the missing mass. In stripping events, on the other hand, where there is
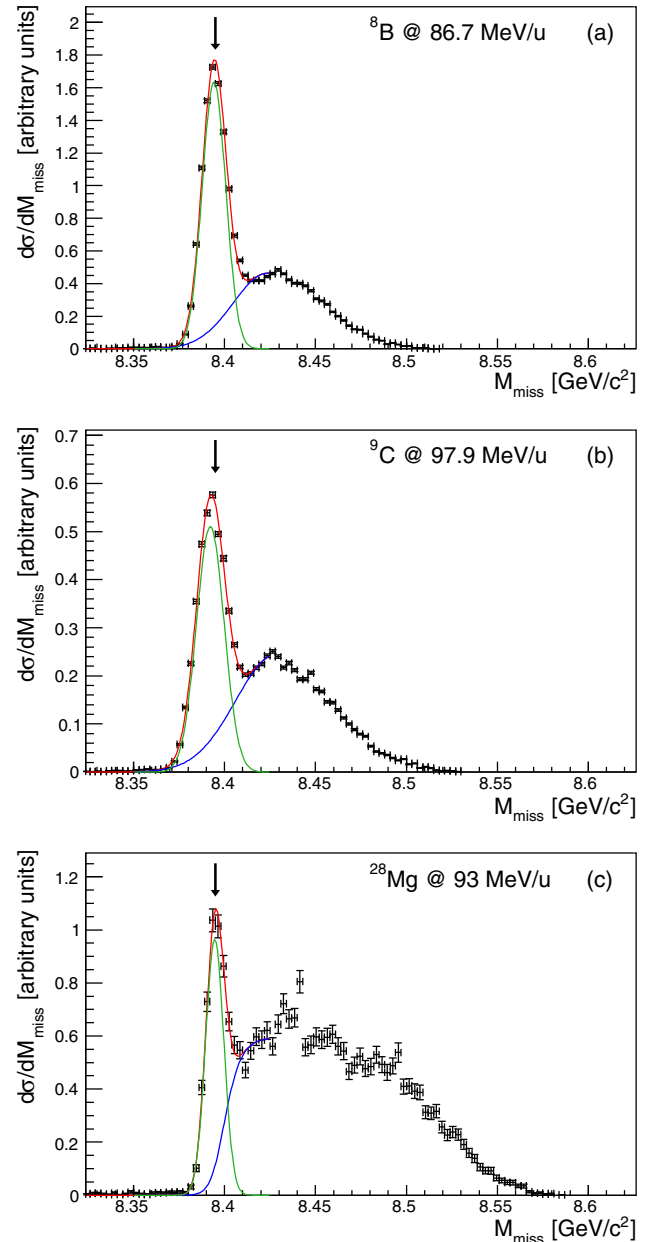


FIG. 1. (Color online) Missing-mass spectra of the one-proton removal reaction residues $^7$Be (a), $^8$B (b), and $^{27}$Na (c) and a proton detected in coincidence. The beam energies are shown in each panel. The arrows show the position of the target mass, $M(^9$Be$)$, and indicate events associated with proton removal by the elastic breakup mechanism. The $^{28}$Mg spectrum is from the current measurement and the $^8$B and $^9$C spectra were extracted from the data sets of Ref. [12].

energy transfer and the target is excited to a greater or lesser degree, the missing mass for such events is higher than the target mass. The continuous broad distributions seen in all panels in Fig. 1 are thus attributed to inelastic breakup events. We note that the larger proton separation energy of the present data set results in the relative contribution from elastic breakup to these proton coincidence events being significantly reduced. This is to be expected for the proton separation energy of

$S_p = 16.79$ MeV, as compared to $S_p = 1.296$ MeV and 0.137 MeV for the $^9$C and $^8$B systems, respectively.

In order to quantify the elastic breakup component to the removal cross section, this missing-mass spectrum is fitted. In the case of the weakly bound $^9$C and $^8$B systems we show a function consisting of two Gaussians following the earlier work of [12]. Numerical values for the relative amount of the elastic breakup cross section discussed later are taken from [12]. The fitting function in the lower panel consists of a Gaussian, to describe the diffraction peak, and a smooth sigmoid step function, to estimate the background from stripping events below $M_{\mathrm{miss}} = 8.41$ GeV/$c^2$:

$$f(M_{\mathrm{miss}}) = \frac{N}{\sqrt{2\pi}\sigma} \exp\left[-\left(\frac{M_{\mathrm{miss}} - M_0}{\sqrt{2}\sigma}\right)^2\right]$$
$$+ N'\left[1 + \exp\left(\frac{M_0' - M_{\mathrm{miss}}}{\sigma'}\right)\right]^{-2}$$

The choice for this shape is motivated by the assumption that the elastic breakup leads to a sharp peak (delta function) at $M_{\mathrm{miss}} = M(^9\mathrm{Be})$ and the inelastic component only contributes for $M_{\mathrm{miss}} > M(^9\mathrm{Be})$. These ideal shapes are then smeared with the experimental resolution. All six parameters of the fit function are left free to vary. Within the uncertainty of the resulting values we find $M_0 = M_0'$ and $\sigma = \sigma'$. The width of the elastic peak, $\sigma$, is in agreement with the expected resolution given by the momentum width of the incoming beam, the differential energy loss in the target, and the energy and angle resolution for protons detected in HiRA. It is more narrow in the case of the proton removal reaction from $^{28}$Mg because of the different optics mode used for the S800. The data for proton removal from $^{28}$Mg shown in Fig. 1(c) were recorded in dispersion-matched mode, while the data sets for the weakly bound light nuclei [Figs. 1(a) and 1(b)] were measured in focused mode—in order to extract the proton angular distribution [12]. In order to extract the elastic contribution to the breakup cross section from Fig. 1, the part of the inelastic contribution leaking into the elastic peak has to be obtained from the fitting procedure. This is the major source of uncertainty in the extraction of the elastic cross section. We have estimated this systematic uncertainty to be 5% by varying the shape of the sigmoid function and by fixing certain parameters in the fit. Before the cross section for the elastic breakup process can be compared to theoretical predictions, additional systematic corrections for misidentification of high- and low-energy protons must be applied because Fig. 1 only contains events with proton kinetic energies between 15 and 120 MeV.

The measured cross section for $^{27}$Na and proton coincidences has to be corrected for the misidentification of particles with very low energies. Protons with kinetic energies below 15 MeV are stopped in the silicon detectors of HiRA and cannot be unambiguously identified. The differential cross sections as a function of the light particle energy therefore shows a step at the energy that is required to punch through the silicon detector. This energy is different for the different light particles. This specific energy loss allows us to extract the number of protons among the unidentified particles and correct the elastic breakup cross section accordingly. At the highest

energies ($E_p \gtrsim 120$ MeV), protons will punch through the silicon as well as the CsI detectors of HiRA with the result that their total kinetic energy is unknown, and they cannot be unambiguously identified using the $\Delta E$-$E$ technique. In order to determine the systematic correction for misidentification of these high-energy protons, the differential cross section as a function of proton kinetic energy is analyzed for the identified protons. This distribution shows a sharp cutoff at $E_p \approx 120$ MeV, which allows us to estimate that 5% of the elastic breakup events result from proton kinetic energies greater than 120 MeV.

After application of these corrections, the elastic breakup fraction of the total one-proton removal cross section can be determined relative to the inclusive cross section for production of $^{27}$Na, discussed above. The value obtained from the $^{27}$Na data set taken in dispersion-matched mode (extracted from Fig. 1 for identified protons and from a similar plot for particles with kinetic energies below the identification threshold) is 11.2(12)% after the aforementioned corrections have been applied. The broad distribution in the missing-mass distribution of Fig. 1, for identified protons, represents 37(2)% of the detected inelastic breakup (stripping) events. While the resolution in the missing-mass spectrum is worse when using the data set taken in focused mode, an elastic breakup fraction of 12.5(17)% was determined. This shows that, even though the two settings have distinct disadvantages, a consistent result is obtained from the two data sets. Finally, these experimental values need to be corrected for the missing angular acceptance of the HiRA array for polar angles $\vartheta < 9°$. As in Ref. [12], this correction is estimated using CDCC calculations. This will be discussed in Sec. IV C.

## IV. THEORETICAL ANALYSIS

### A. Shell-model input

As stated, the measurements made are inclusive with respect to all bound final states of $^{27}$Na, whose ground state has $S_n = 6.73$ MeV. Shell-model calculations using the USD $sd$-shell effective interaction [17] are used to compute the $^{28}$Mg ground state and the $^{27}$Na final states and one-proton removal spectroscopic factors ($C^2S$). This shell-model proton removal strength is predominantly to just three final states, with observed counterparts: the $5/2^+$ ground state, with $C^2S = 3.137$, an almost degenerate $3/2^+$ (14-keV) state with $C^2S = 0.124$, and a $1/2^+$ (1630-keV) state with $C^2S = 0.304$. Additional small fragments of $5/2^+$, $3/2^+$, and $1/2^+$ strength are distributed over many excited states below the 6.73-MeV first neutron threshold. Thus, as stated earlier, the ground state to ground state removal is expected to be the dominant transition. However, given the inclusive nature of the measurements, in the following calculations, when comparisons are made with the data, we sum these small fragments of strength into the spectroscopic factors used for the three states above. These become $C^2S(5/2^+) = 3.289$, $C^2S(3/2^+) = 0.262$, and $C^2S(1/2^+) = 0.330$ and are the values shown in Table I. Their sum, of 3.88, effectively exhausts the spectroscopic sum rule. Given the large ground state to ground state $S_p$ of 16.79 MeV, assigning the same

TABLE I. Shell-model states of $^{27}$Na and their spectroscopic factors (see text) for one-proton removal from $^{28}$Mg from the USD effective interaction [17]. We show the theoretical proton removal cross sections to each final state (for 93 MeV/nucleon projectiles on a $^9$Be target), their elastic and inelastic breakup components, and the overall predicted fraction (%) of elastic breakup events (Elas.). The predicted summed $C^2S$ of 3.88 to these bound configurations essentially exhausts the maximum available strength.

| $J^\pi$ | $E_x$ (MeV) | $C^2S$ | $\sigma_{th}^{inel}$ (mb) | $\sigma_{th}^{elas}$ (mb) | $\sigma_{th}$ (mb) | Elas. (%) |
|---|---|---|---|---|---|---|
| $5/2^+$ | 0.000 | 3.289 | 38.75 | 8.47 | 47.22 | 17.9 |
| $3/2^+$ | 0.014 | 0.262 | 2.95 | 0.64 | 3.59 | 17.8 |
| $1/2^+$ | 1.630 | 0.330 | 3.86 | 0.92 | 4.78 | 19.3 |
| Sum | | 3.88 | 45.56 | 10.03 | 55.59 | 18.0 |

(smaller) excitation energy to these multiple small fragments will overestimate slightly their cross section contribution, but this has a very small effect on the inclusive cross section and a negligible effect on the fraction of cross section due to elastic breakup.

### B. Eikonal model calculations

This shell-model structure information is now used with the eikonal dynamical model [5,6] to make theoretical predictions for the inclusive one-proton removal cross section at 93 MeV per nucleon and for its components from the elastic and inelastic breakup mechanisms. More specifically, we follow precisely (i) the framework for the construction of the proton- and residue-target optical potentials and their eikonal $S$ matrices, from the assumed $^9$Be target and $^{27}$Na Hartree-Fock (HF) densities and (ii) constraints on the geometries of the bound-state radial overlap functions of the proton using analogous and consistent HF calculations for $^{28}$Mg, as are described in detail in Ref. [3]. All bound proton wave functions are calculated in Woods-Saxon wells with diffuseness $a_0 = 0.7$ fm and a spin-orbit potential strength of $V_{so} = 6.0$ MeV. The reduced radius parameters $r_0$ consistent with the HF constraints are 1.285, 1.322, and 1.205 fm for the $1d_{5/2}$, $1d_{3/2}$, and $2s_{1/2}$ orbitals, respectively. The effective proton separation energies used in comparing with the data are determined from the empirical $S_p$ and the shell-model excitation energies in Table I.

Based on these reaction inputs, Fig. 2 shows the calculated dependence of the percentage fractional contribution of the elastic breakup (diffraction) mechanism to the proton removal cross section for pure $1d_{5/2}$, $1d_{3/2}$, and $2s_{1/2}$ single-proton orbitals as a function of the proton separation energy (from $S_p = 0.05$ through 20 MeV). The actual contributions from each shell-model final state, weighted by their spectroscopic factors, at the physical $S_p$ are shown in Table I. The theoretical cross sections $\sigma_{th}$ include the $[A/(A-1)]^N$ center-of-mass correction factor to the shell-model spectroscopic factors [18], with $N = 2$ for these $sd$-shell orbitals. We see that, from these eikonal model calculations, the computed theoretical elastic breakup fraction is 18%. In Sec. IV D we will investigate minor corrections to these presented conventional eikonal
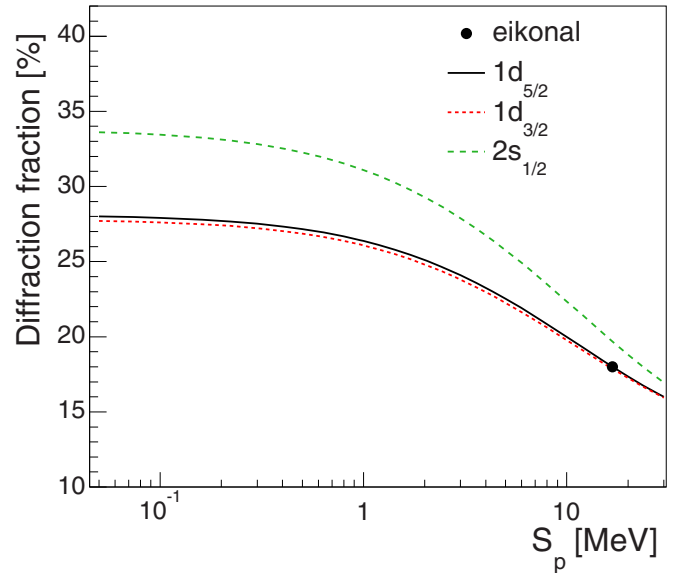


FIG. 2. (Color online) Computed fractional contribution (%) of the elastic breakup (diffraction) reaction mechanism to the proton removal cross section as a function of the proton separation energy. The lines show the predictions of the eikonal model for proton removal from $1d_{5/2}$ (solid black), $1d_{3/2}$ (dotted red), and $2s_{1/2}$ (dashed green) orbitals. The theoretical prediction, 18%, when using spectroscopic factors calculated from the shell model (see text and Table I), is shown by the filled black circle.

calculations resulting from some flux leading to transitions of the proton between bound states and not to the breakup continuum. First we discuss the measured and calculated inclusive cross section values and also comment on the separation energy dependence of the calculated elastic breakup fractions as are shown by the lines in Fig. 2.

#### 1. Inclusive cross section

The measured inclusive cross section of 36(1) mb can be compared to the calculated cross section of 55.6 mb. The asymmetry of the neutron and proton Fermi surfaces in $^{28}$Mg, based on their separation energies and the dominance of the ground-state transition, means (in the notation of [3]) that $\Delta S = 8.29$ MeV for one-proton removal. The cross section ratio $R_s = \sigma_{exp}/\sigma_{th}$ is therefore 0.65(2). This value is consistent with the systematics of this cross section ratio with $\Delta S$, referred to in the introduction and shown in the figures of Refs. [3,4].

#### 2. Separation energy dependence

In the previously studied weakly bound proton cases, $^9$C and $^8$B [12], of order one third of the proton removal cross section was due to elastic breakup. The calculated elastic breakup fractions for removal from the active $1d_{5/2}$, $1d_{3/2}$, and $2s_{1/2}$ $sd$-shell proton orbitals of $^{28}$Mg all show a similar dependence as the proton separation energy $S_p$ is allowed to change by a factor of 40, from 0.5 to 20 MeV, in Fig. 2. Thus, the overall percentage of diffraction events has little sensitivity to the details of the shell-model calculations and

their spectroscopic factors. As is expected, the elastic breakup fraction decreases with increasing separation energy but at nothing like the rate expected were the dependencies as $1/\sqrt{S_p}$, which would suggest a reduction of more than a factor of 6. This is confirmation, see, e.g., Fig. 3 of Ref. [3], that the reaction is not asymptotic. We consider the physically dominant $1d_{5/2}$ case. Here, the elastic fraction falls by less than a factor of 2, from 28% to 17%, over the range of separation energies and these changes correlate much more closely with the weaker sensitivity of the rms radius, $r_{\rm sp}$, of the orbital to $S_p$ (which ranges from 4.20 to 3.22 fm). For the calculations shown in Fig. 2 the $1d_{5/2}$ elastic breakup fraction is found to scale as $r_{\rm sp}^{3/2}$ to better than 5% over the range of $S_p$ considered. It would be of interest to examine this dependence further, experimentally, with data on nearby $sd$-shell nuclei having a range of $S_p$.

### C. Angular acceptance correction

Given the expected and calculated dominance of the ground state to ground state $5/2^+$ transition, a CDCC calculation for the elastic breakup from a $1d_{5/2}$ proton orbit is used to estimate those breakup events that are unobserved due to the angular acceptance of HiRA, as were used for the lighter projectile data [12]. The CDCC calculations are performed using the direct reactions code FRESCO [19]. The calculations describe $^{28}$Mg in terms of its dominant $^{27}$Na plus proton ground-state configuration and include $^{27}$Na $+ p$ breakup states for configurations with relative orbital angular momenta $\ell = 0$–4 and relative energy up to 30 MeV. For each breakup partial wave this continuum energy interval is divided into 15 bins, while the coupled channels calculations include projectile-target partial waves up to total angular momentum 300 and use a matching radius of 50 fm. The theoretical optical potentials, bound-state radial wave functions, and other inputs used were in common with those used in the eikonal calculations of Sec. IV B. The model space required for a stable calculation is far more demanding than in the weakly bound, light projectile cases and it was not clear that the calculation and the derived observables were fully converged. Thus, the correction should be interpreted as indicative and not fully quantitative.

Within this CDCC model space, the exclusive laboratory frame elastic breakup differential cross section $(d^3\sigma/dE_p d\Omega_p d\Omega_r)$ (see, e.g., Ref. [20]) was computed. This differential cross section, fully integrated over the proton and residue final-state variables, was then compared with that integrated over the experimental acceptances for which the $^{27}$Na residue travels in the forward direction with $\Delta\Omega_r = 21$ msr and $\vartheta_p = 9°$–$56°$; see also [12] for further details. Based on this three-body CDCC model analysis we estimate that 15% of the elastic breakup events will be unobserved by the detector (polar angle) acceptances of the present experimental setup. This provides an approximate angular acceptance correction factor to the measured (lower limit) elastic breakup fractions. If applied to the fraction measured in focused mode [12.5(17)%] presented in Sec. III], which is better suited since the angles of protons can be determined with high accuracy, a deduced elastic breakup fraction of 14.7(20)%
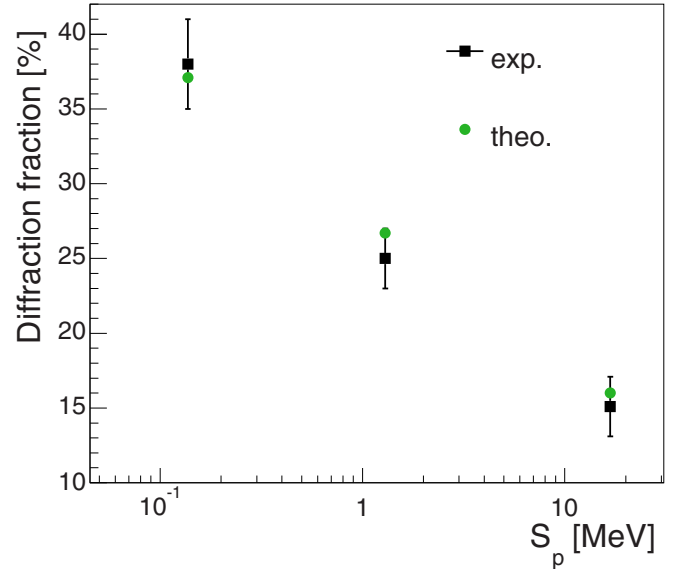


FIG. 3. (Color online) Experimental (black squares) and theoretical (green circles) fractional contribution (%) of the elastic breakup (diffraction) reaction mechanism to the proton removal cross section as a function of the proton separation energy. In addition to the present study the figure also shows the previously measured cases of weakly bound proton removals from $^9$C and $^8$B [12].

is obtained. This experimental value is shown in Fig. 3. If instead the value measured in the dispersion-matched mode is corrected for the proton angle acceptance, the resulting elastic breakup fraction amounts to 13.2(14)%.

### D. Bound-state transition corrections

The eikonal model calculations presented above follow the formalism of Ref. [5], specifically, Eqs. (2) and (4)–(8), and use potential and size parameters as described in Sec. IV B. These calculations take only the $i = 0$ term in the calculation of the elastic breakup part of the single-particle cross section in Eq. (6) of Ref. [5]. The expression for the elastic breakup cross section to a given residue final state $c$, which is assumed to be a spectator in the reaction, is written as the following integral over the projectile center-of mass impact parameters $\vec{b}$:

$$\sigma_{\rm sp}^{\rm elas}(c) = \frac{1}{2I+1} \int d\vec{b} \left[ \sum_M \langle \phi_{IM}^c | \, |\mathcal{S}_c \mathcal{S}_p|^2 \, |\phi_{IM}^c\rangle \right.$$

$$\left. - \sum_{i\gamma m', M} |\langle \phi_{\gamma m'}^{cj'}(i) | \mathcal{S}_c \mathcal{S}_p | \phi_{IM}^c\rangle|^2 \right],$$

where $\mathcal{S}_c$ and $\mathcal{S}_p$ are the residue- and proton-target elastic scattering $S$ matrices and $\gamma$ denotes the core spin substate. Here, $\phi_{IM}^c$ is the (normalized) angular momentum coupled configuration of the core state and the proton in the projectile ground state, so, for $^{28}$Mg($I^\pi = 0^+$), $\phi_{00}^c \equiv [c \otimes n(\ell s)j]_{00}$. The $\phi_{\gamma m'}^{cj'}(i)$ represent product states of the particular residue

(spectator core) state $c\gamma$ and a proton in a configuration $[n'(\ell's)j'm']$. The $i = 0$ term represents the $n'\ell'_{j'} \equiv 1d_{5/2}$, $1d_{3/2}$, or $2s_{1/2}$ proton bound state, respectively, for the $5/2^+$, $3/2^+$, and $1/2^+$ residue final states of importance here, the same $n\ell_j$ orbital as appears in $\phi^c_{00}$. Extra terms, with $i \neq 0$, represent other possible bound proton single-particle configurations with respect to the core state $c$. So, in the elastic breakup calculations presented in Table I, truncated to $i = 0$, we have assumed that all projectile-target interactions that remove the proton from the given entrance channel configuration, $1d_{5/2}$, $1d_{3/2}$, or $2s_{1/2}$, lead to continuum states of $^{27}$Na and the proton and elastic breakup. Thus proton single-particle transitions to other bound states of the proton and the residue $c$ are neglected. As is clear from the structure of the equation for $\sigma^{\rm elas}_{\rm sp}(c)$, the inclusion of such transitions will necessarily reduce the calculated elastic breakup cross section.

The role of such transitions between bound configurations was calculated and found to have a very minor effect on the single-particle cross sections (stripping plus diffraction) for light neutron-rich nuclei (of order 3% in Ref. [5]). This was due in part to the importance and dominance of the stripping mechanism, even for weakly bound nucleons, seen in Fig. 2, and to the likelihood of a small number of such bound $i \neq 0$ configurations when removing a weakly bound nucleon of an excess species. Such terms have since been neglected in comparisons with data.

Since the present work involves a direct and exclusive measurement of the elastic breakup contribution and a well-bound proton, it is opportune to estimate this effect in this case. In addition to the $i = 0$ terms, the set of possible bound configurations ($i = 1,2,3$) may involve proton $1d_{5/2}$, $1d_{3/2}$, $2s_{1/2}$, and $1f_{7/2}$ configurations. Whether there is bound $1f_{7/2}$ proton strength with respect to the core states is unclear. A spherical HF calculation for $^{28}$Mg using the Skyrme SkX interaction [21] does bind the $\pi 1f_{7/2}$ orbital by $\approx 1$ MeV. The reduced radius parameter $r_0$ consistent with HF constraints is 1.209 fm for this $7/2^-$ orbital.

The eikonal calculations of $\sigma^{\rm elas}_{\rm sp}(c)$ have been repeated. In addition to the $i = 0$ calculations of Table I, reproduced and denoted 0 in Table II, we show there the results for calculations that include bound transitions assuming a $1d_{5/2}$, $1d_{3/2}$, and $2s_{1/2}$ space (denoted $ds$) and also when including an assumed $1f_{7/2}$ bound state at the calculated HF separation energy of 0.84 MeV (denoted $dsf$). Table II shows, in each case, the theoretical partial and inclusive removal cross sections, calculated as in Table I, and the computed percentage contribution from elastic breakup. As must be the case, this elastic breakup cross section fraction is reduced as the space of possible proton transitions to bound states is increased, since these transitions remove flux hitherto assumed to lead to breakup. However, as was found in Ref. [5], the effect on the inclusive proton removal cross section is small ($\lesssim 3\%$) and within the errors for typical data sets involving well-bound nucleon removal.

The calculations suggest, however, that the eikonal model percentage of elastic breakup events shown in Table I (i.e., calculation 0) and in Fig. 2, of 18%, is too large. The most reliable estimate based on these extended calculations, summarized in Table II, is that the elastic fraction is 16%,

TABLE II. Theoretical cross sections for one-proton removal from $^{28}$Mg at 93 MeV/nucleon on a $^9$Be target. Calculations use the USD shell-model spectroscopic factors of Table I. The predicted percentages of elastic breakup events are shown in the columns headed Elas. The three sets of calculations, labeled 0, $ds$, and $dsf$, result from eikonal model calculations that neglect (case 0) and include (cases $ds$ and $dsf$) the effects of proton single-particle transitions between bound states upon the elastic breakup calculation. Full details are given in the text of Sec. IV D.

| $J^\pi$ | $E_{\rm x}$ (MeV) | $\sigma_{\rm th}$ (mb) 0 | Elas. (%) 0 | $\sigma_{\rm th}$ (mb) $ds$ | Elas. (%) $ds$ | $\sigma_{\rm th}$ (mb) $dsf$ | Elas. (%) $dsf$ |
|---|---|---|---|---|---|---|---|
| $5/2^+$ | 0.000 | 47.22 | 17.9 | 46.14 | 16.0 | 45.71 | 15.2 |
| $3/2^+$ | 0.014 | 3.59 | 17.8 | 3.51 | 16.0 | 3.50 | 15.6 |
| $1/2^+$ | 1.630 | 4.78 | 19.3 | 4.60 | 16.0 | 4.52 | 14.6 |
| Sum | | 55.59 | 18.0 | 54.25 | 16.0 | 53.73 | 15.2 |

since the additional assumption of bound $\pi 1f_{7/2}$ states is speculative. Figure 3 shows that these theoretical values are in good agreement with that, 14.7(20)%, deduced from the present more exclusive measurement.

For completeness, Fig. 2 also shows the calculated and experimental values for the earlier-studied cases, of proton removal from $^9$C and $^8$B [12]. For all three cases, spanning a wide range in separation energies, theoretical calculations agree with the experimentally determined fractional contribution of the elastic breakup reaction mechanism.

## V. SUMMARY AND CONCLUSIONS

In summary, we have studied the one-proton removal reaction from the neutron-rich $sd$-shell nucleus $^{28}$Mg at the intermediate energy of 93 MeV per nucleon. Light charged particles were detected in coincidence with the fast $^{27}$Na residues, allowing the missing-mass spectrum to be measured. The distribution of events in the missing-mass spectrum allowed the determination of the relative contribution of elastic breakup to the removal reaction in this case of a well-bound proton. This deduced fraction of elastic breakup events was found to be in good agreement with the eikonal model calculations of the reaction yields within the experimental and theoretical uncertainties, extending the earlier-reported agreement for removal reactions involving weakly bound protons.

[1] T. Nakamura *et al.*, Phys. Rev. Lett. **83**, 1112 (1999).

[2] T. Aumann and T. Nakamura, Phys. Scr. **T152**, 014012 (2013).

[3] A. Gade *et al.*, Phys. Rev. C **77**, 044306 (2008).

[4] J. A. Tostevin, Prog. Theor. Phys. (Suppl.) **196**, 275 (2012).

[5] J. A. Tostevin, Nucl. Phys. A **682**, 320 (2001).

[6] P. G. Hansen and J. A. Tostevin, Annu. Rev. Nucl. Part. Sci. **53**, 219 (2003).

[7] A. Bonaccorso and D. M. Brink, Phys. Rev. C **38**, 1776 (1988).

[8] F. Flavigny, A. Obertelli, A. Bonaccorso, G. F. Grinyer, C. Louchart, L. Nalpas, and A. Signoracci, Phys. Rev. Lett **108**, 252501 (2012).

[9] A. Bonaccorso and G. F. Bertsch, Phys. Rev. C **63**, 044604 (2001).

[10] A. García-Camacho, R. C. Johnson, and J. A. Tostevin, Phys. Rev. C **71**, 044606 (2005).

[11] M. Zinser *et al.*, Nucl. Phys. A **619**, 151 (1997).

[12] D. Bazin *et al.*, Phys. Rev. Lett. **102**, 232501 (2009).

[13] D. J. Morrissey, B. M. Sherrill, M. Steiner, A. Stolz, and I. Wiedenhoever, Nucl. Instrum. Methods Phys. Res. B **204**, 90 (2003).

[14] D. Bazin, J. A. Caggiano, B. M. Sherrill, J. Yurkon, and A. Zeller, Nucl. Instrum. Methods Phys. Res. B **204**, 629 (2003).

[15] M. Wallace *et al.*, Nucl. Instrum. Methods Phys. Res. A **583**, 302 (2007).

[16] K. Wimmer *et al.*, Phys. Rev. C **85**, 051603 (2012).

[17] B. H. Wildenthal, Prog. Part. Nucl. Phys. **11**, 5 (1984).

[18] A. E. L. Dieperink and T. L. de Forest Jr., Phys. Rev. C **10**, 543 (1974).

[19] I. Thompson, computer code FRESCO, http://www.fresco.org.uk/index.htm; see also I. J. Thompson, Comput. Phys. Rep. **7**, 167 (1988). .

[20] J. A. Tostevin, F. M. Nunes, and I. J. Thompson, Phys. Rev. C **63**, 024617 (2001).

[21] B. A. Brown, Phys. Rev. C **58**, 220 (1998).